

Nonlinear generation of extreme-ultraviolet radiation in atomic hydrogen using electromagnetically induced transparency

G. Z. Zhang, D. W. Tokaryk, and B. P. Stoicheff

Department of Physics, University of Toronto and Ontario Laser and Lightwave Research Centre, Toronto, Ontario, Canada M5S 1A7

K. Hakuta

Department of Applied Physics and Chemistry and Institute for Laser Science, University of Electro-Communications, Chofu, Tokyo 182, Japan

(Received 2 December 1996)

Sum-frequency generation enhanced by electromagnetically induced transparency (EIT) has been extended to the production of extreme ultraviolet (XUV) radiation in the range 97.3–92.6 nm from np - $1s$ transitions ($n=4-8$) in atomic hydrogen. Pulsed radiation was generated by strong coupling of the np and $2s$ levels with laser radiation at Balmer wavelengths, and simultaneously (weaker) coupling of the $2s$ and $1s$ levels by two-photon resonance with 243-nm laser radiation. Investigations were carried out over a range of laser intensities and products of interaction length and atomic density (NL). As the product NL increased, the XUV intensities were greatly enhanced by EIT, and at high NL values, the spectral distributions of some of the generated signals were found to be distorted by the presence of molecular hydrogen. Calculated profiles, modified to incorporate the effects of nearby molecular resonances, were shown to be in good agreement with the observed spectra. [S1050-2947(97)05206-2]

PACS number(s): 42.65.Ky, 42.50.Hz, 42.50.Gy, 32.80.Fb

I. INTRODUCTION

Electromagnetically induced transparency (EIT) is a phenomenon that arises when two atomic levels are strongly coupled, either by decay to a common level [1] or by the application of an electromagnetic field [2] to the bare states to create two closely spaced states that decay to a common lower level. Under these conditions, resonance absorption for the transition from the lower state to the dressed state is strongly suppressed [3] because of quantum interference between the two transition pathways, while emission from the dressed states is resonantly enhanced. In addition to its application in lasing without inversion [1–4], refractive index control [5], and propagation through normally opaque media [6], EIT has been shown to enhance nonlinear optical processes such as four-wave frequency mixing [7]. Specifically, the nonlinear susceptibility $\chi^{(3)}$ and the associated emission benefit from constructive quantum interference on resonance, while the linear susceptibility $\chi^{(1)}$ and absorption are suppressed.

In past work in this laboratory, atomic hydrogen has been used as the medium in which to explore EIT-enhanced nonlinear generation in the vacuum ultraviolet (VUV) region. Hakuta and co-workers [7] examined the enhancement of second harmonic generation by using 243-nm laser radiation for the $2s$ - $1s$ two-photon resonance while coupling the $2s$ and $2p$ levels with a strong dc electric field. In their work, conducted at low atomic number density, they observed the effects of EIT and enhancement of the generated intensity at 121.6 nm (the $2p$ - $1s$, Lyman- α transition) arising from the increased nonlinear susceptibility. At higher density and interaction length, the peak SH (second harmonic) power was 6 W, an increase in efficiency by 3 orders of magnitude from that with $E_{dc}=0$. Zhang and co-workers [8,9] used the same

general scheme with a strong laser field at 656 nm to couple the $2s$ and $3p$ levels, thus generating EIT-enhanced VUV radiation at 102.6 nm (the $3p$ - $1s$, Lyman- β transition). They also examined the effect of increasing atomic number density and laser-atom interaction length on the generated intensity. In all of these experiments with EIT in atomic hydrogen, detailed calculations showed that observations were in good agreement with the available theory.

In the present paper, we extend the earlier studies of EIT-enhanced four-wave mixing in atomic hydrogen to the generation of extreme ultraviolet (XUV) radiation by strong coupling of the $2s$ and high np ($n>3$) levels with intense Balmer radiation. While the effects of electromagnetic coupling to levels near the ionization limit and the continuum beyond were examined, with emission observed from dressed states up to $n\sim 35$, the intensity decreased markedly with higher n , so that EIT was demonstrated only up to $n=8$ because of limited coupling-laser power. Here, we will describe our observations obtained with coupling of the $2s$ with the $4p$ and $8p$ levels using 486.1 and 389.0-nm Balmer radiation, resulting in emission at 97.3 and 92.6 nm, respectively. The first generation of 97.3-nm radiation in atomic hydrogen by four-wave mixing was reported by Troshin, Chebotayev, and Chernenko in 1978 [10], before the concept of EIT had been introduced. In the present work, experiments were carried out under various conditions of coupling power, detuning from resonance, and at small and large values of the product of atomic density and interaction length. The medium contained molecular as well as atomic hydrogen, and nearby transitions of molecular hydrogen affected the generated spectra. The effects of molecular transitions on the dispersion and absorption of the medium were analyzed and included in calculations of the spectral profiles. Such effects were first observed by Katsuragawa, Zhang, and

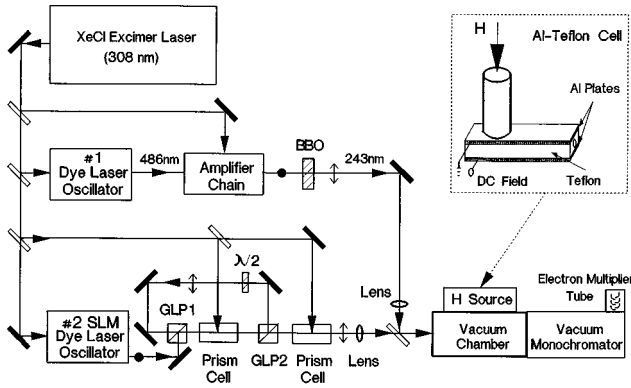


FIG. 1. Schematic diagram of the experimental arrangement. BBO is the β -barium borate crystal used for second-harmonic generation of 243-nm radiation, and GLP1 and GLP2 are Glan-laser prisms. In the inset is shown the Al-Teflon cell used to increase the atomic hydrogen-laser interaction length to ~ 5 cm.

Hakuta for generation of 103-nm radiation with strong coupling in atomic hydrogen [11].

II. EXPERIMENT DETAILS

The present experiments were carried out using apparatus and experimental techniques (Fig. 1) similar to those described earlier [9]. A XeCl excimer laser (Lumonics TE-861M-4) generating 308-nm radiation at 8-MW peak power in 34-ns pulses was used to pump two dye laser systems. One was a tunable dye laser (home made [12]) generating 486-nm radiation with peak powers of ~ 150 kW in pulses of 10-ns duration and a 0.19-cm^{-1} linewidth, full width at half maximum (FWHM). After two amplifying stages, the output was focused with a 300-mm focal length lens into a β -barium borate (BBO) crystal to produce 243-nm radiation. This linearly polarized radiation, of 0.03-mJ energy in pulses of 6-ns duration, was used for coupling the $2s\text{-}1s$ two-photon resonance. The second dye laser was a tunable, single-longitudinal-mode (SLM) laser [13] (Lumonics Hyper DYE-SLM) to provide $np\text{-}2s$ coupling radiation with a linewidth of 0.02-cm^{-1} (FWHM). Several different dyes were used in the SLM laser to access the various $np\text{-}2s$ transitions with Balmer radiation in the range 364–486 nm. The SLM laser power was increased by passing the beam through two Bethune-prism amplifiers, and enhanced further by sending the laser pulse twice through the first amplifier using two Glan-prisms and a half-wave plate (Fig. 1). After amplification, the laser output was 1–2 mJ per pulse for all laser wavelengths (as measured with a Gentec ED200 pyroelectric joulemeter), and linearly polarized in the same direction as the 243-nm beam. The pulse profiles were near-Gaussian, spatially and temporally, with durations varying from 9 to 16 ns (FWHM) due to the different gain saturations of the various dyes in the oscillator and amplifier chain.

The coupling and 243-nm beams were focused by quartz lenses having focal lengths of 500 and 250 mm, respectively. The beams were spatially overlapped by a dichroic mirror, temporally overlapped by adjusting the length of a delay sidearm in the SLM path, and then sent into a vacuum chamber for interaction with the atomic hydrogen. The beam di-

ameters (FWHM) were ~ 0.45 mm for the coupling beam and ~ 0.21 mm for the 243-nm beam over a 5–6-cm length of the interaction region. Laser wavelengths were calibrated against optogalvanic spectra obtained from a U-Ne hollow cathode lamp. An étalon with a free spectral range of 1-cm^{-1} and a finesse of 20 at 486 nm was used as a frequency marker and as a monitor of the mode quality of the SLM laser radiation.

Atomic hydrogen was produced in a Wood's discharge tube made of Pyrex, typically operated at 2000 V dc, with 0.5 Torr of hydrogen, and then was passed through a Pyrex finger (7 cm long, at right angles to the discharge tube) to a simple slit [9] or a long sample cell, illustrated in Fig. 1. The slit (1 mm wide and 3 mm long), was used in experiments conducted at low values of the product NL , where N is the atomic hydrogen density and L is the laser-hydrogen interaction length. The cell was designed to channel the hydrogen along the laser path, thereby increasing the interaction length to ~ 50 mm. It was constructed of Teflon side-walls (3 mm thick) sandwiched between two aluminum plates for collection of laser-produced photoelectrons and photoions that were used to monitor EIT (and connected to the Pyrex finger by a 3-cm-long Teflon-lined tube). A quartz window was sealed at the input end, and an exit aperture of 1.5 mm was drilled through the Teflon at the other end. Both slit and cell were suspended in a vacuum chamber evacuated with a high-capacity diffusion pump (TM-Vacuum Products, Model TM4MM).

XUV radiation generated by the nonlinear mixing process passed through an evacuated tube to a vacuum monochromator (McPherson 225), and was detected by an electron multiplier tube (Thorn EMI 226EM). Photoions produced by the laser beams were collected from the slit source with a pair of electrodes (at electric fields $E_{dc} < 100$ V/cm), and from the Al-Teflon cell directly with the aluminum plates ($E_{dc} \sim 30$ V/cm). The XUV radiation, and photoion, optogalvanic, and étalon signals were processed by boxcar integrators (Stanford Research Systems 245), then digitized and stored in a computer for analysis.

III. RESULTS AND DISCUSSION

A. XUV generation with EIT in the low- NL limit

The generation of XUV radiation and of photoions (proportional to the absorption rate of the generated radiation) was first carried out at values of $NL \sim 10^{13}\text{--}10^{14}\text{-cm}^{-2}$ using the slit source. This provided an interaction length $L = 0.3$ cm and an estimated atom density $N \sim 10^{14}\text{-cm}^{-3}$ (assumed from earlier experiments with the same discharge source [9]). In Fig. 2 are shown the results for XUV and photoion generation at the $4p\text{-}1s$ (97.3-nm) transition, obtained by applying laser radiation at 486 nm to couple the $4p$ and $2s$ levels, while detuning ($\Delta\omega_{21}$) the two-photon laser frequency from the $2s\text{-}1s$ resonance. Spectra are given for three different values of the coupling Rabi frequency Ω_{42} , defined as usual as $\mu_{42}E/\hbar$. Here μ_{42} is the $4p\text{-}2s$ transition dipole moment, and E is the amplitude of the electric field associated with the coupling-laser beam. The resonant electromagnetic coupling creates a pair of dressed states, energetically centered at the $4p$ level and separated by

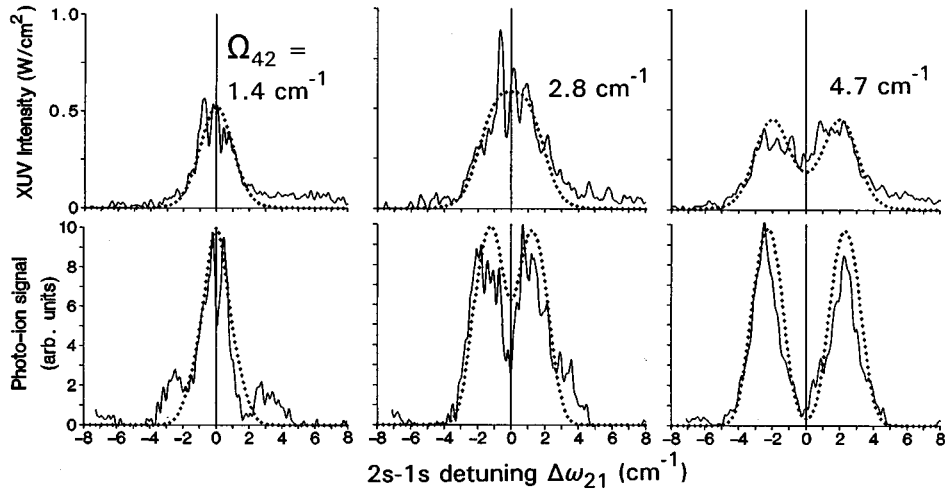


FIG. 2. XUV radiation (near 97.3 nm) and photoion signals from the slit source (with $NL \sim 0.6 \times 10^{14} \text{ cm}^{-2}$) vs detuning of the two-photon laser frequency from the $2s$ - $1s$ resonance. The coupling-laser frequency was set to the $4p$ - $2s$ transition at 486.1 nm. Calculated (----) and observed (—) spectra are shown for three different Rabi frequencies Ω_{42} . The vertical scale for the XUV signals is based on calculated intensities at the exit end of the slit. The photoion signals are normalized for each Rabi frequency.

the Rabi frequency Ω_{42} . As the Rabi frequency is increased, the spectral breadth of the photoion signal increases, until at sufficiently strong coupling, 2.8 cm^{-1} , two peaks are resolved at the dressed-state positions, and their separation provides a measure of the coupling Rabi frequency. At the highest coupling power available ($\Omega_{42} = 4.7 \text{ cm}^{-1}$), the ion signal at the resonance center is suppressed to nearly zero, indicating that the EIT is well developed.

Calculations of the expected ion signals were carried out using the expressions and procedures discussed in Ref. [9] and the results are plotted in Fig. 2. Values for the transition dipole moments were calculated from available data [14], and photoionization cross sections for the $2s$ and $4p$ levels were obtained from [15]. Good agreement with the experimental data was obtained for a Doppler breadth of 2.0 cm^{-1} , and NL set to $0.6 \times 10^{14} \text{ cm}^{-2}$ (in qualitative agreement with the estimated density of earlier work [16]), when the results were normalized at each value of the Rabi frequency, as shown in Fig. 2. However, comparison of absolute values when normalized at $\Omega_{42} = 4.7 \text{ cm}^{-1}$ leads to experimental values at the lower Rabi frequencies, which are only about half those given by theory, as also found in earlier work at low- NL values [8,9].

The XUV spectra shown in Fig. 2 broaden with increasing coupling-laser intensity (and increasing Rabi frequency), and split into two components at the highest Rabi frequency of $\Omega_{42} = 4.7 \text{ cm}^{-1}$. Under this strong-coupling condition, the generated XUV intensity at resonance center is approximately half of the peak value of the two dressed components but not zero, in contrast to the zero ion signal at resonance. As is well known [7], this results from the constructive interference for the nonlinear susceptibility $\chi^{(3)}$ (which determines the rate of emission) and from destructive interference for $\chi^{(1)}$. Simulations of the XUV-generated signals were performed using the expressions for EIT-enhanced nonlinear mixing given in Ref. [7]. The agreement with experimental data is satisfactory, despite the low intensity and noise of the XUV signals.

The low intensity of the $4p$ - $1s$ signal at 97.3 nm, relative to that of the $3p$ - $1s$ transition at 102.6 nm, studied in the earlier work under similar conditions [8,9], can be partially attributed to the larger laser beam diameters used in the present work, and thus to weaker coupling, but mainly to the smaller dipole moment for the 97.3-nm transition. At relatively low values of NL , such as those used here, the generated XUV intensity is proportional to the square of the nonlinear susceptibility $\chi^{(3)}$, which in turn is proportional to the product $\mu_{n2}\mu_{n1}$ of the np - $2s$ and np - $1s$ dipole transition moments. The square of this product is about an order of magnitude smaller for the $4p$ - $1s$ transition than it is for the $3p$ - $1s$ transition. Moreover, in the earlier work, a Rabi frequency as high as 15 cm^{-1} was possible, but here the coupling-laser power limited the observations to 4.7 cm^{-1} because of the lower value of μ_{42} .

With coupling of the $2s$ level to higher np levels, the XUV signals decreased markedly, and for $8p$ - $2s$ coupling (at 389 nm), resulting in the $8p$ - $1s$ transition at 92.6 nm, the intensity was too low for meaningful analysis. This observation was not surprising, given that the square of the product of dipole moments involving the $8p$ level is $<1\%$ of the already small $4p$ product. While the photoion signal was observed, and splitting was seen at the highest achievable Rabi frequency, $\Omega_{82} = 3.2 \text{ cm}^{-1}$ in Fig. 3(a), the shallow decrease in ion signal on resonance indicates that reduced absorption from EIT was just beginning to develop at the strongest available $8p$ - $2s$ coupling power.

B. XUV generation in the high- NL limit

To increase the intensity of the generated XUV radiation, experiments were conducted with the Al-Teflon cell at a value of $NL \sim 10^{15} \text{ cm}^{-2}$, a factor of ~ 10 over that obtained with the slit. Figure 4 shows the photoion- and XUV-generated signals obtained with the Al-Teflon cell versus detuning of the two-photon laser frequency for several different coupling Rabi frequencies at the $4p$ - $2s$ transition. Note that the signals are much narrower than with the slit source (Fig.

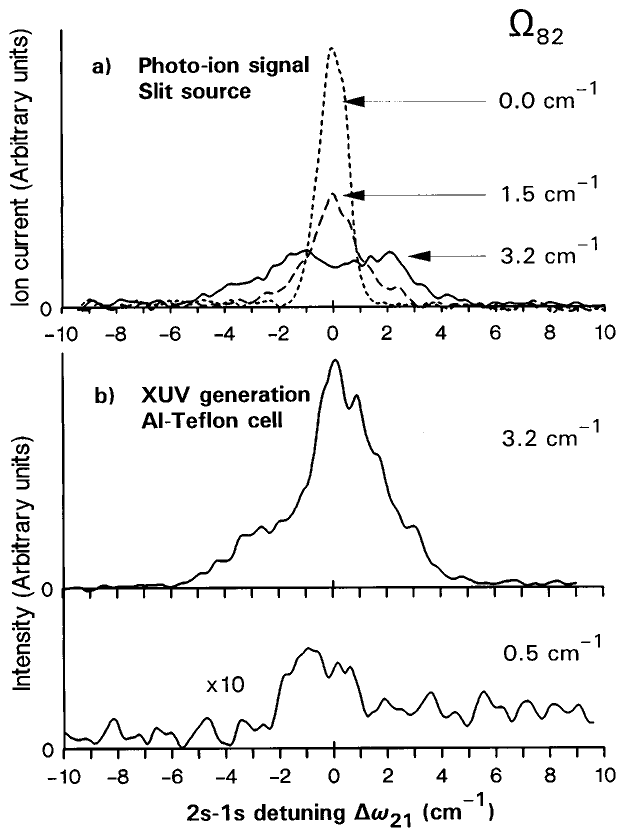


FIG. 3. (a) Photoion signals from the slit source (with $NL \sim 0.6 \times 10^{14} \text{ cm}^{-2}$) vs detuning of the two-photon laser frequency from the $2s-1s$ resonance, with the coupling-laser frequency set to the $8p-2s$ transition at 389.0 nm. Spectra are shown for three values of the Rabi frequency Ω_{82} . (b) XUV radiation generated using the Al-Teflon cell ($NL \sim 10^{15} \text{ cm}^{-2}$) vs $2s-1s$ detuning, with the coupling-laser wavelength set at 389.0 nm. Spectra are shown for two values of the Rabi frequency Ω_{82} (with the vertical scale of the lower trace increased by a factor of 10 over that of the upper trace).

2), a result arising partly from colder atoms after collisions in the longer connecting tube from discharge to cell and in the long cell itself, and mainly from the high NL . When the coupling Rabi frequency exceeds the Doppler width of about 1.3 cm^{-1} , the XUV intensity at the resonance center is the main feature in the spectrum, while the intensity of the two Autler-Townes components is much lower. This is in contrast to the slit data, where the intensity at the resonance center was only about half that of the two components. At the maximum coupling Rabi frequency of 4.2 cm^{-1} , the XUV peak in Fig. 4 is slightly shifted from the resonance center, and the minimum in the photoion signal is no longer located at the resonance center. Moreover, an unexpected component appears in both spectra at a frequency detuning $\Delta\omega_{21}$ of about $+3.2 \text{ cm}^{-1}$, while no matching feature is seen at a detuning of -3.2 cm^{-1} . It is also noted that the photoion spectrum exhibits a pronounced asymmetry in both peaks.

Recently, Katsuragawa, Zhang, and Hakuta [11] reported on the observation of similar anomalies in the $3p-1s$ VUV-generated spectrum. They explained their observations by including the effects of nearby transitions of molecular hydrogen on the susceptibility $\chi^{(1)}$ of the mixed H-H₂ medium. The authors noted that the nearest molecular transition, the $P(1)$ line in the 6-0 vibrational band of the $B^1\Sigma_u^+ - X^1\Sigma_g^+$ electronic transition (the Lyman system), lies 20 cm^{-1} to the red of the $3p-1s$ atomic hydrogen transition; four other lines from the same vibrational band lie within $\pm 230 \text{ cm}^{-1}$. In the present work, we find from the tables of Dabrowski [17], that the $R(1)$ line in the 11-0 band of the same electronic transition lies only 11 cm^{-1} to the red of the $4p-1s$ transition, and that the $R(0)$ and $P(1)$ lines are also nearby, at 85 cm^{-1} to the blue and 58 cm^{-1} to the red, respectively. The close proximity of these molecular lines, particularly the $R(1)$ line, to the atomic hydrogen transition, suggests that molecular effects will play an even stronger role in the $4p-1s$ spectrum than in that of the $3p-1s$ transition.

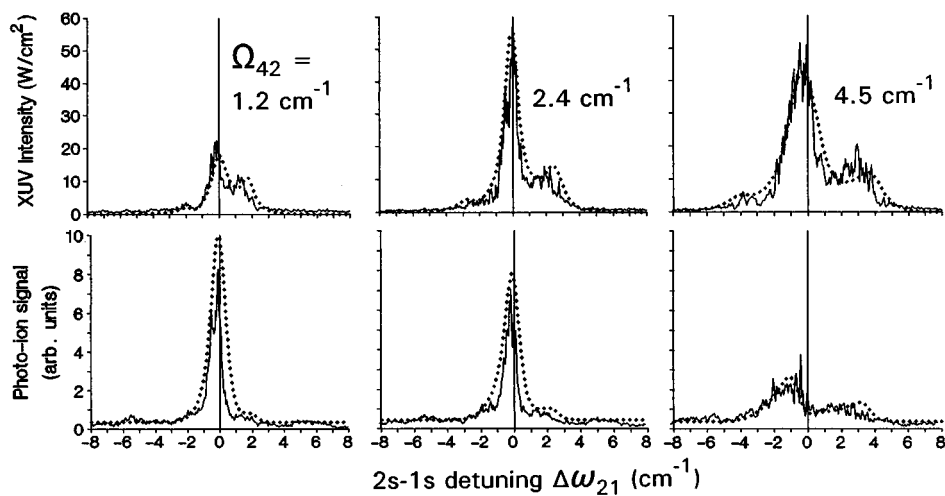


FIG. 4. XUV radiation (near 97.3 nm) and photoion signals using the Al-Teflon cell ($NL \sim 10^{15} \text{ cm}^{-2}$) vs detuning $\Delta\omega_{21}$ of the laser frequency. The coupling laser frequency was set to the $4p-2s$ transition at 486.1 nm. Calculated (----) and observed (—) spectra are shown for Rabi frequencies $\Omega_{42} = 1.2, 2.4,$ and 4.5 cm^{-1} . Simulations were carried out with Doppler breadths of 1.45, 1.75, and 2.35 cm^{-1} , respectively, with widths for H₂ set to $2^{-1/2}$ of these values. The vertical scale for XUV signals is based on calculated intensities at the exit end of the cell.

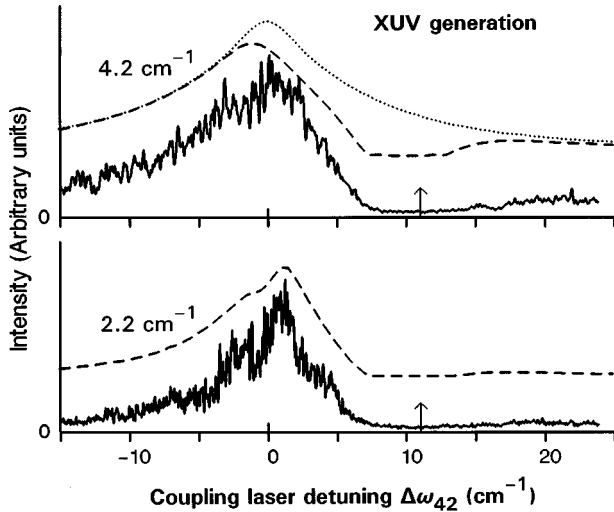


FIG. 5. XUV radiation (near 97.3 nm) using the Al-Teflon cell ($NL \sim 10^{15} \text{ cm}^{-2}$) vs detuning of the coupling-laser frequency for the $4p$ - $2s$ resonance, and with the 243-nm radiation set to the $2s$ - $1s$ two-photon transition. Spectra are shown for two values of the Rabi frequency Ω_{42} . Calculated (---) spectra taking into account the effects of the nearby molecular H_2 transition (\dagger) are compared with observed spectra (—). A calculated spectrum (····) without consideration of the effects of molecular dispersion is shown for $\Omega_{42} = 4.2 \text{ cm}^{-1}$. (The calculated spectra are shifted vertically for clarity, and the vertical scales are the same for the two Rabi frequencies.)

Following Katsuragawa, Zhang, and Hakuta [11], we have added to the expression for the linear susceptibility $\chi^{(1)}$ terms χ_M (of the usual form) describing the dispersion and absorption arising from nearby molecular transitions:

$$\chi_M = (N_J \mu_J^2 / \hbar \epsilon_0) \{ (\omega_J - \omega - i\Gamma)^{-1} + (\omega_J + \omega + i\Gamma)^{-1} \}, \quad (1)$$

where N_J is the number density of H_2 in the J th rotational level of the ground vibronic state, μ_J represents the dipole moment of a particular transition involving the J th level, Γ is the total decay rate of the upper state, ω is the frequency of the applied field, and ω_J is the frequency of the molecular transition. A term of this form for the nearest molecular transition, namely, the $R(1)$ line, was added to the calculation of $\chi^{(1)}$. The more distant transitions were found to make negligible contributions. Values for the upper-level lifetimes Γ are known [18], and values for μ_J were assessed from tables of oscillator strengths for the Lyman bands [19], following the procedures outlined by Thorne [20]. The molecular number density in the cell could not be readily determined, since neither the dissociation efficiency nor the post-discharge pressure could be measured. However, the population of the ground-state rotational levels was assumed to follow a Boltzmann distribution at 400 K, taking into account the nuclear spin statistics.

The calculated values for the XUV and photoion signals (with the modified expression for $\chi^{(1)}$ included), are plotted along with the observed spectra in Fig. 4. In the simulation, the interaction length was set at 5 cm, and the average number density of atomic hydrogen was assumed as the slit value of $2 \times 10^{14} \text{ cm}^{-3}$. The total number density of H_2 was varied

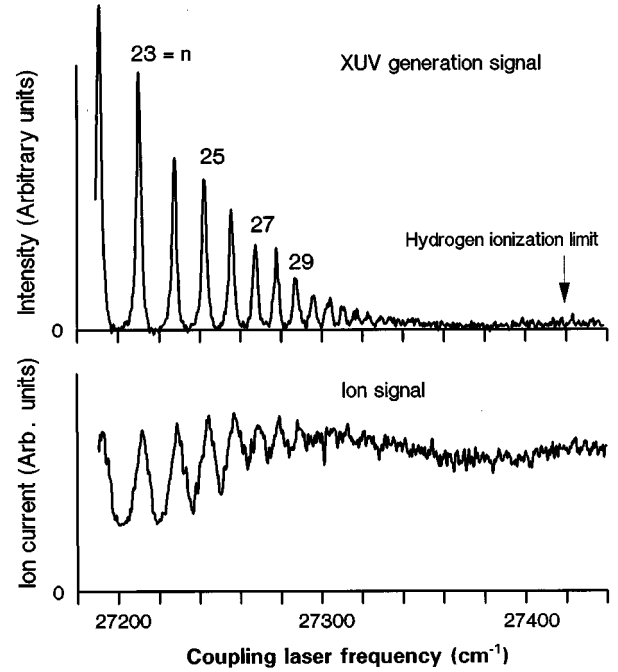


FIG. 6. XUV radiation (near 91.2 nm) and photoion signals using the Al-Teflon cell ($NL \sim 10^{15} \text{ cm}^{-2}$) vs the coupling laser frequency with the 243-nm laser radiation set to the $2s$ - $1s$ two-photon resonance. The coupling laser scan extends from 27 190 to 27 440 cm^{-1} , that is from about the $22p$ - $2s$ transition and beyond the ionization limit (measured from the $2s$ state).

until a reasonable fit to the data was achieved; a value of $10 \times 10^{14} \text{ cm}^{-3}$ gave acceptable results. The relative intensities of XUV and photoion signals for the three Rabi frequencies were in best agreement when the effective Doppler widths (1.45, 1.75, and 2.35 cm^{-1}) for atomic hydrogen were assumed to increase with Rabi frequency, as discussed in [8]. Figure 4 shows that good agreement between simulation and experiment is obtained at each value of the Rabi frequency for both the XUV and photoion signals. Moreover, the observed position and intensity of the extra peak, and asymmetries in the spectra at the higher Rabi frequencies are adequately reproduced, indicating that the effects of molecular hydrogen have been taken into account correctly.

The effects of molecular hydrogen on the nonlinear generation process are even more pronounced when the two-photon laser frequency is fixed at the $2s$ - $1s$ transition while the coupling laser is scanned, as shown in Fig. 5 for two different Rabi frequencies. At the 11-0 band, $R(1)$ resonance position, a broad intensity minimum is observed, indicating that the generated radiation is almost completely absorbed by the coexisting H_2 . Also shown for the larger Rabi frequency is a comparison of simulations with and without the molecular effects. Clearly, the simulation correctly represents the observed spectrum only when the nearby molecular transition is taken into account.

Similar experiments on XUV generation with strong coupling of the $2s$ level to np levels up to $10p$, were carried out using the Al-Teflon cell. With the higher NL values obtained in the cell, the intensity of the XUV radiation was greatly enhanced compared to the intensity obtained using the slit

source, but there was a rapid decrease with increasing n value. Here, we will briefly describe the results involving the $8p$ level (with coupling of $8p$ - $2s$ levels by 389-nm radiation), since EIT was not noticeably developed at the higher levels with the available laser power. The generated signal versus two-photon frequency detuning for low and high values of the applied Rabi frequency ($\Omega_{82}=0.5$ and 3.2 cm^{-1}) is shown in Fig. 3(b). The XUV signal is barely perceptible for weak coupling, and becomes more intense in the presence of the EIT produced by stronger coupling. Again, asymmetry in the XUV line shape is noted, particularly for negative values of two-photon laser detuning. This is attributed to the presence of the $R(2)$ line in the 17-0 band of the H_2 Lyman bands [17], only 11 cm^{-1} on the high-frequency side of the $8p$ - $1s$ transition.

Experiments on XUV and photoion generation were also conducted on high-Rydberg levels by tuning the coupling laser between $27\,190$ and $27\,440\text{ cm}^{-1}$ with the two-photon laser frequency fixed on resonance with the $2s$ level. This scanning range covered Rydberg levels with $n > 22$ [21], and extended into the ionization limit above the $2s$ state. Charts of the observed XUV and photoion signals vs coupling laser frequency are shown in Fig. 6. While XUV radiation is produced when the coupling laser is tuned to an np resonance (up to $n \sim 35$), the ion signal is enhanced rather than suppressed at the resonance centers. Clearly, the coupling power is far from sufficient to induce transparency in these high-Rydberg transitions, so the generated XUV radiation is reabsorbed by other atoms, which are then ionized by photons from the coupling and two-photon lasers. A small amount of generated radiation appears as a background up to and beyond the ionization limit.

IV. CONCLUSIONS

This work extends studies on EIT-enhanced four-wave mixing in atomic hydrogen to the generation of XUV radiation ($< 100\text{ nm}$) in the Lyman series, $np \rightarrow 1s$, with $n > 3$. The studies show that despite a monotonic decrease in np - $1s$ and np - $2s$ transition probabilities with increasing n , EIT can still be observed up to at least $n = 8$ with the laser powers available from our apparatus. In other words, coupling was achieved between levels separated by $\sim 26\,000\text{ cm}^{-1}$, and should be possible for more distant levels. However, to achieve reasonable XUV intensities, the atomic density-interaction length product NL had to be increased by a factor of ~ 10 relative to earlier work on the $2p$ - $1s$ and $3p$ - $1s$ VUV transitions performed with the same atomic hydrogen source. For high-Rydberg levels near the ionization limit, weak nonlinear generation was still observed, although the available coupling laser powers were insufficient to produce EIT for these transitions.

We have also observed strong distortions in the profiles of the $4p$ - $1s$ XUV and photoion spectra as a result of nearby molecular hydrogen resonances. Such resonances affect the linear susceptibility $\chi^{(1)}$ of the mixed H-H_2 medium, and therefore disturb the nonlinear generation process. It was possible to simulate the observed spectra by including in calculations of the susceptibility a molecular dispersion term arising from a known molecular line only 11 cm^{-1} from the atomic Lyman- γ line at 97.3 nm .

ACKNOWLEDGMENTS

This research was supported by the Natural Sciences and Engineering Research Council of Canada (NSERCC), Technology Ontario, and the University of Toronto.

-
- [1] S. E. Harris, Phys. Rev. Lett. **62**, 1033 (1989); M. O. Scully, S.-Y. Zhu, and A. Gavrielides, *ibid.* **62**, 2813 (1989).
- [2] A. Imamoglu and S. E. Harris, Opt. Lett. **14**, 1344 (1989).
- [3] K.-J. Boller, A. Imamoglu, and S. E. Harris, Phys. Rev. Lett. **66**, 2593 (1991); J. E. Field, K. H. Hahn, and S. E. Harris, *ibid.* **67**, 3062 (1991).
- [4] A. S. Zibrov, M. D. Lukin, D. E. Nikonov, L. Hollberg, M. O. Scully, V. L. Velichansky, and H. G. Robinson, Phys. Rev. Lett. **75**, 1499 (1995); G. G. Padmandu, G. R. Welch, I. N. Shubin, E. S. Fry, D. E. Nikonov, M. D. Lukin, and M. O. Scully, *ibid.* **76**, 2053 (1996).
- [5] M. O. Scully, Phys. Rev. Lett. **67**, 1855 (1991); M. Jain, A. J. Merrian, A. Kasapi, G. Y. Yin, and S. E. Harris, *ibid.* **75**, 4385 (1995); A. Kasapi, G. Y. Yin, M. Jain, and S. E. Harris, Phys. Rev. A **53**, 4547 (1994); M. Jain, G. Y. Yin, J. E. Field, and S. E. Harris, Opt. Lett. **18**, 998 (1993).
- [6] S. E. Harris, Phys. Rev. Lett. **72**, 52 (1994); J. H. Eberly, M. L. Pons, and H. R. Haq, *ibid.* **72**, 56 (1994); A. Kasapi, M. Jain, G. Y. Yin, and S. E. Harris, *ibid.* **74**, 2447 (1995).
- [7] S. E. Harris, J. E. Field, and A. Imamoglu, Phys. Rev. Lett. **64**, 1107 (1990); K. H. Hahn, D. A. King, and S. E. Harris, *ibid.* **65**, 2777 (1990); K. Hakuta, L. Marmet, and B. P. Stoicheff, *ibid.* **66**, 596 (1991); K. Hakuta, L. Marmet, and B. P. Stoicheff, Phys. Rev. A **45**, 5152 (1992); K. Hakuta, L. Marmet, and B. P. Stoicheff, in *Laser Spectroscopy X*, edited by M. Ducloy, E. Giacobino, and G. Camy (World Scientific, Singapore, 1991), p 301.
- [8] G. Z. Zhang, K. Hakuta, and B. P. Stoicheff, Phys. Rev. Lett. **71**, 3099 (1993); G. Z. Zhang, M. Katsuragawa, K. Hakuta, R. I. Thompson, and B. P. Stoicheff, Phys. Rev. A **52**, 1584 (1995).
- [9] R. I. Thompson, B. P. Stoicheff, G. Z. Zhang, and K. Hakuta, Quantum Opt. **6**, 349 (1994); Appl. Phys. B **60**, 129 (1995).
- [10] B. I. Troshin, V. P. Chebotaev, and A. A. Chernenko, Pis'ma Zh. Eksp. Teor. Fiz. **27**, 293 (1978) [JETP Lett. **27**, 273 (1978)].
- [11] M. Katsuragawa, G. Z. Zhang, and K. Hakuta, Opt. Commun. **129**, 212 (1996).
- [12] P. R. Herman, P. E. LaRocque, R. H. Lipson, W. Jamroz, and B. P. Stoicheff, Can. J. Phys. **63**, 1581 (1985).
- [13] M. G. Littman, Opt. Lett. **3**, 138 (1978); Appl. Opt. **23**, 4465 (1984); G. Z. Zhang and K. Hakuta, Opt. Lett. **17**, 997 (1992).
- [14] E. U. Condon and G. H. Shortley, *Theory of Atomic Spectra* (Cambridge University Press, Cambridge, 1987), p 136.
- [15] A. Burgess, Mem. R. Astron. Soc. **69**, 1 (1965).
- [16] L. Marmet, K. Hakuta, and B. P. Stoicheff, J. Opt. Soc. Am. B **9**, 1038 (1992).
- [17] I. Dabrowski, Can. J. Phys. **62**, 1639 (1984).

- [18] A. C. Allison and A. Dalgarno, *J. Quant. Spectrosc. Radiat. Transf.* **9**, 1543 (1969).
- [19] A. C. Allison and A. Dalgarno, *Mol. Phys.* **19**, 567 (1970).
- [20] A. P. Thorne, *Spectrophysics*, 2nd ed. (Chapman and Hall, London, 1988), Chap. 12.
- [21] H. Rottke, H. Zacharias, and K. H. Welge, in *Laser Techniques for Extreme Ultraviolet Spectroscopy*, edited by T. J. McIlrath and R. R. Freeman (AIP, New York, 1982), p. 402.